Acta Crystallographica Section D
Biological Crystallography
ISSN 0907-4449

X-ray structure of azide-bound fully oxidized cytochrome *c* oxidase from bovine heart at 2.9 Å resolution

Ming Jie Fei,[a] Eiki Yamashita,[a] Noriko Inoue,[a] Min Yao,[a] Hiroshi Yamaguchi,[a] Tomitake Tsukihara,[a] Kyoko Shinzawa-Itoh,[b] Ryosuke Nakashima[b] and Shinya Yoshikawa[b]*

[a]Institute for Protein Research, Osaka University, 3-2 Yamada-oka, Suita 565, Japan, and [b]Department of Life Science, Himeji Institute of Technology and CREST, Japan Science and Technology Corporation (JST), Kamigohri Akoh, Hyogo 678-12, Japan

Correspondence e-mail: yoshi@sci.himeji-tech.ac.jp

Received 14 September 1999
Accepted 7 February 2000

PDB Reference: cytochrome *c* oxidase, 1ocz.

Two azide ions were identified, one between the Fe and Cu atoms in the O_2-reduction site and the other at the transmembrane surface of the enzyme, in the crystal structure of the azide-bound form of bovine heart cytochrome *c* oxidase at 2.9 Å resolution. Two geometries, a μ-1,3 type geometry between the Fe and Cu atoms and a terminal geometry on the Fe atom, are equally possible for an azide ion in the O_2-reduction site. The other azide molecule was hydrogen bonded to an amide group of an asparagine and a hydroxyl group of tyrosine in a μ-1,1 type geometry. The antisymmetric infrared bands arising from these azide ions, which show essentially identical intensity [Yoshikawa & Caughey (1992), *J. Biol. Chem.* **267**, 9757–9766], strongly suggest terminal binding of the azide to Fe. The electron density of all three imidazole ligands to Cu_B was clearly seen in the electron-density map of the azide-bound form of bovine heart enzyme, in contrast to the crystal structure of the azide-bound form of the bacterial enzyme [Iwata *et al.* (1995), *Nature (London)*, **376**, 660–669], which lacks one of the three imidazole ligands to Cu_B.

1. Introduction

Cytochrome *c* oxidase is the terminal enzyme in the respiratory chain of most aerobic organisms. It contains two haems and two copper sites as the redox-active metal sites. The two metal sites, haem a_3 and Cu_B, form the O_2-reduction site (Ferguson-Miller & Babcock, 1996). Electrons from cytochrome *c* are transferred to the O_2-reduction site through the other two metal sites, Cu_A and haem *a* (Ferguson-Miller & Babcock, 1996). Bovine heart cytochrome *c* oxidase is the largest terminal oxidase, composed of 13 different protein subunits with a molecular mass of about 210 kDa (Kadenbach *et al.*, 1983; Tsukihara *et al.*, 1996). Because of its physiological importance and intriguing catalytic reaction, the enzyme has been studied extensively since its discovery (Warburg, 1924).

Iwata *et al.* (1995) have determined the crystal structure of the bacterial enzyme in the azide-bound fully oxidized state. They found that one of the three imidazole ligands to Cu_B lacks electron density, suggesting a mobile structure in the imidazole ligand. Before the crystal structure appeared, a mechanism (the 'histidine cycle') had been proposed for proton pumping of cytochrome *c* oxidase, in which one of the imidazole ligands to Cu_B changes its conformation and protonation state depending on the oxidation state of the O_2-reduction site (Wikström *et al.*, 1994). Thus, the mobile structure of His325 (His290 in bovine heart enzyme) led to the proposal that this histidine is the site of proton pumping (Iwata *et al.*, 1995). On the other hand, the crystal structure of

the fully oxidized bovine heart cytochrome *c* oxidase free from azide (Tsukihara *et al.*, 1995) has three imidazole ligands to Cu_B. Therefore, we have determined the crystal structure of the azide-bound fully oxidized enzyme isolated from bovine heart at 2.9 Å resolution. In contrast to the bacterial enzyme, all three histidine ligands to Cu_B are present in the crystal structure. Part of the results given here have been published in a preliminary form (Yoshikawa *et al.*, 1998).

2. Experimental and structure determination

2.1. Preparation of crystals

Single crystals of the azide-bound fully oxidized form were prepared by soaking single crystals of the fully oxidized form, prepared as described previously (Yoshikawa *et al.*, 1998), for 4 d at 277 K in 5 m*M* sodium azide, 40 m*M* sodium phosphate buffer pH 6.8 containing 0.2%(*w*/*v*) *n*-decyl-β-D-maltoside and 5%(*w*/*v*) polyoxyethylene glycol 4000 (Sigma).

2.2. Intensity data acquisition

X-ray diffraction data were collected at 285 ± 2 K using a Weissenberg camera for macromolecules (Sakabe, 1983) with monochromated X-rays of wavelength 1.0 Å at the Photon Factory, Tsukuba, Japan. 1° oscillation frames were taken at a crystal-to-camera distance of 429.7 mm. The exposure time of each frame was 180 s. The diffraction beam path to the detector was filled with helium gas in order to reduce the X-ray absorption by air and the background arising from X-ray scattering by air. Diffraction data were recorded on 400 × 200 mm imaging plates (Fuji). Each imaging plate was read by a Fuji BASS-2000 system in 100 µm steps.

128 oscillation frames, obtained from three crystals, were processed with the program *DENZO* (Otwinowski & Minor, 1997). They were then scaled using the program *SCALEPACK* (Otwinowski & Minor, 1997). The intensity data obtained are summarized in Table 1, together with three heavy-atom derivative data sets used for the crystal structure analysis of the oxidized form. A total of 133 922 independent reflections were obtained at 2.9 Å resolution from 561 728 observed reflections, with an $R_{\rm merge}$ of 0.078, an averaged redundancy of 4.2 and a completeness of 85.7%.

2.3. Crystal structure determination

A Patterson map was calculated with $|F_o|^2$ coefficients in order to inspect the translational symmetry within the asymmetric unit.

Three heavy-atom derivatives of the fully oxidized form were used for phase determination of the azide-bound form using the multiple isomorphous replacement (MIR) method (Green *et al.*, 1954). The initial heavy-atom sites of each derivative were determined by calculating a $(F_{PH} - F_P)^2$ difference Patterson map. Refinement of the heavy-atom parameters with the program *MLPHARE* (Otwinowski, 1991) from the *CCP*4 program suite (Collaborative Computational Project, Number 4, 1994) and difference Fourier synthesis were alternated repeatedly to search for minor peaks and to improve the initial estimates of the heavy-atom parameters. Solvent flattening (Wang, 1985) coupled with histogram matching (Zhang & Main, 1990) and non-crystallographic symmetry (NCS) averaging (Buehner *et al.*, 1974; Argos & Rossmann, 1976) by means of the program *DM* from the *CCP*4 program suite were applied to extend the MIR phases. In order to incorporate NCS averaging into the density-modification procedure, a molecular envelope was generated for each monomer manually, as it was very difficult to determine the interface between the two monomers automatically. A correlation coefficient, $\{\sum(\rho_1 - \langle\rho_1\rangle)(\rho_2 - \langle\rho_2\rangle)\big/ \sum[(\rho_1 - \langle\rho_1\rangle)^2(\rho_2 - \langle\rho_2\rangle)^2]^{1/2}\}$, was calculated at each step of NCS averaging in order to monitor the structural similarity of two independent monomers in the electron-density distribution, where $\langle\rho_i\rangle$ is the averaged electron density of monomer *i*. The resultant map of the density-modification procedure is referred to as the MIR/*DM* map.

The initial model for the *X-PLOR* refinement (Brünger *et al.*, 1987) was derived from the structure of the oxidized form and was refined by simulated annealing, positional refinement and *B*-factor refinement. The refined structure was manually revised in the MIR/*DM* map after each cycle of *X-PLOR* refinement. The structure was confirmed by using $(2F_o - F_c)$ omit maps at the final stage of the refinement. The restraint parameters used in *X-PLOR* were the stereochemical parameters of Engh & Huber (1991). NCS restraints were included

Table 1
Data-collection statistics.

Intensity data collection.

Compound	Native	$IrCl_6$ (I)	$IrCl_6$ (II)	CH_3HgCl
Resolution (Å)	100.0–2.9	100.0–3.0	100.0–3.0	100.0–3.0
Reflections				
Observed	561728	319358	381828	328484
Independent	133932	119549	111957	107859
Competeness (%)	85.7	86.3	93.0	88.3
Merging *R*†	0.078	0.090	0.062	0.085
$R_{\rm iso}$‡		0.073	0.057	0.090
$R_{\rm Cullis}$§		0.86	0.86	0.79
Phasing power¶		0.63	0.57	0.86

Completeness of native data in each resolution range.

Resolution range (Å)	Completeness (%)
6.25–4.96	96.9
4.96–4.33	97.2
4.33–3.94	94.9
3.94–3.65	92.1
3.65–3.44	86.9
3.44–3.27	80.1
3.27–3.12	75.7
3.12–3.00	70.2
3.00–2.90	66.3

† Merging $R = \sum_h \sum_i |I(h,i) - \langle I(h)\rangle| / \sum_h \sum_i I(h,i)$, where $I(h,i)$ is the intensity value of the *i*th measurement of *h* and $\langle I(h)\rangle$ is the corresponding mean value of $I(h)$ for all measurements; the summation is over the reflections with $I/\sigma(I) > 1.0$. ‡ $R_{\rm iso} = \sum|F_{PH} - F_P|/\sum F_{PH}$, where F_{PH} and F_P are the derivative and the native structure-factor amplitudes, respectively. § $R_{\rm Cullis} = \sum ||F_{PH} - F_P| - F_H({\rm calc})|/\sum|F_{PH} - F_P|$, where F_H(calc) is the calculated heavy-atom structure factor. The summation is over the centric reflections only. ¶ Phasing power is the r.m.s. isomorphous difference divided by the r.m.s. residual lack of closure.

in the refinement process. The manual rebuilding of the model was repeated according to the MIR/*DM* map and/or the $(2F_o - F_c)$ map calculated with Fourier coefficients of $(2F_o - F_c)\exp(i\alpha_c)$, where α_c was a calculated phase angle from the structural model. Some amino-acid residues which did not fit well to the MIR/*DM* map were rebuilt successfully in the $(2F_o - F_c)$ map.

3. Results

3.1. Crystal and intensity data

The crystals of the azide-bound enzyme belonged to the orthorhombic space group $P2_12_12_1$, with unit-cell parameters a = 189.2 (6), b = 210.6 (5), c = 178.5 (6) Å. The crystallographic asymmetric unit contained one dimer, with a molecular weight of 420 kDa, a V_m of 4.4 Å^3 Da^{-1} and a solvent content of about 72% according to Matthews' equation (Matthews, 1968).

3.2. Crystal structure determination

The Patterson map calculated with $|F_o|^2$ coefficients had a prominent peak in the asymmetric unit which was attributed to a pseudo-twofold axis parallel to the c axis. The peak position in the Patterson map representing a vector between two pseudo-twofold axes related by a crystallographic 2_1 symmetry was in the same position as that of the oxidized enzyme. Consequently, the isomorphism between the azide-bound and the fully oxidized forms was confirmed. Nine heavy-atom sites for the Ir (I) derivative, one for the Ir (II) derivative and 27 for the Hg derivative were determined by the difference Patterson method coupled with *MLPHARE* refinement. The final statistics of the MIR phasing are given in Table 1. After the density-modification procedure coupled with NCS averaging, the correlation coefficient was improved from 0.547 to 0.879 and the free R factor (Brünger, 1992) for 5% of the reflections in each shell was reduced from 0.523 to 0.271. Membrane proteins often produce crystals containing large amounts of solvent molecules, as is the case in bovine heart cytochrome *c* oxidase. Therefore, solvent flattening should be very useful in phase refinement of the X-ray diffraction data from many membrane proteins. NCS averaging was also powerful in improving the quality of the electron-density map.

An R factor of 0.193 and a free R factor of 0.255 were obtained after 15 cycles of *X-PLOR* refinement for 133 932 independent reflections at 2.9 Å resolution. Most of the 3560 amino-acid residues, two haems *a*, two haems a_3, six Cu atoms, two Zn atoms, two Mg atoms, 16 phospholipids, six phosphatidyl glycerols, four cholic acids and two decyl maltosides were located in the crystallographic asymmetric unit and were fully consistent with the crystal structure of the fully oxidized enzyme. The root-mean-square deviations from ideal values were 0.015 Å for bond lengths and 2.2 ° for bond angles. Of the 3058 non-glycine and non-proline residues, 98.9% were in the most favourable and favourable regions (Morris *et al.*, 1992) of the final Ramachandran (φ, ψ) plot (Ramachandran & Sasisekharan, 1968) and only 0.3% were in the disallowed region. These criteria indicate that the refinement was successful.

3.3. Overall structure

The azide-bound fully oxidized cytochrome oxidase was in a dimeric state related by a pseudo-twofold axis in the asymmetric unit of dimensions 90 × 150 × 115 Å. Each monomer of the azide form could be superposed on the corresponding monomer of the fully oxidized form, with an averaged r.m.s. displacement of 0.66 Å for C^α atoms. The distances between metal centres, Cu_A—Fe_a of 20.7 Å, Cu_A—Fe_{a3} of 23.2 Å, Fe_a—Fe_{a3} of 13.4 Å and Cu_A—Zn of 65.2 Å, coincided with those of the oxidized form within estimated errors (Tsukihara *et al.*, 1996). Therefore, azide binding to the fully oxidized form did not affect the overall three-dimensional structure at this resolution.

3.4. Structure of the O_2-reduction site

In contrast to the bacterial enzyme (Iwata *et al.*, 1995), the electron density for all three histidine ligands to Cu_B (His240, His290 and His291) was clearly seen in our MIR/*DM* map of the azide-bound fully oxidized enzyme from bovine heart, as shown in Fig. 1. The MIR/*DM* electron density of His240 and Tyr244 was consistent with that of the fully oxidized enzyme at 2.3 Å resolution (Yoshikawa *et al.*, 1998), in which a covalent linkage between an imidazole N atom of His240 and an *ortho*-phenol C atom of Tyr244 was detectable.

In the azide form, continuous electron density between Cu_B and Fe_{a3} was obvious in the MIR/*DM* electron density map at 2.9 Å resolution. A difference Fourier map calculated with $(F_o - F_c)\exp(i\alpha_c)$ coefficients also showed a large peak between Cu_B and Fe_{a3} (Fig. 2). Three trial structures for an azide molecule at the O_2-reduction site were refined under different restraining conditions, as shown in Table 2. A refinement under the restraining conditions of 2.07 Å for the Fe_{a3}—N_1 distance and 1.90 Å for the Cu_B—N_3 distance converged to give the azide as a bridging structure with typical coordination bonds at both ends of the molecule. Another refinement under the restraining conditions of 2.07 Å for the Fe_{a3}—N_1 distance converged with the azide as a bridging structure, with a typical coordination bond Fe_{a3}—N_1 and a weak interatomic interaction between Cu_B and N_3. These refinements generated no significant residual density at the O_2-reduction site in $(F_o - F_c)$ maps. That is, the two resultant structures are equally possible at 2.9 Å resolution. The third refinement, under the restraining condition of 1.90 Å for the Cu_B—N_3 distance, provided a structure in which N_1 was far from Fe_{a3} and bulky residual density higher than 2σ occurred between Fe_{a3} and N_1 in the $(F_o - F_c)$ map. Consequently, this third structure was unlikely. The above analysis indicated that terminal bonding to Fe_{a3} and bridging bonding between Fe_{a3} and Cu_B were equally possible. The distance between Cu_B and Fe_{a3} was 5.2 Å, compared with 4.9 Å in the fully oxidized form (Yoshikawa *et al.*, 1998). The position of Cu_B is affected by the

ligand binding as well as the oxidation state of the metal sites, whereas the position of Fe_{a3} is essentially insensitive.

3.5. An azide on the transmembrane surface

An azide bound to the protein on a non-metal site was identified with the two difference Fourier maps calculated with $(F_{azi} - F_{oxi})\exp(i\alpha_{oxi})$ and $(F_{azi} - F_c)\exp(i\alpha_c)$, where F and α are the structure amplitude and phase angle, and the suffixes 'azi' and 'oxi' represent the azide and oxidized forms, respectively. An atomic model of azide fitted well to the difference densities, with higher than 4σ density at the molecular surface in the middle of the transmembrane part, as shown in Fig. 3. At one end the azide was hydrogen bonded to an amide group of Asn422 and a hydroxyl group of Tyr379.

Table 2
Restraining conditions of *X-PLOR* refinement and refined structures of azide molecule at the O_2-binding site.

	Restraints		Refined structures		
Models	$Fe_{a3}-N_1$† (Å)	Cu_B-N_3† (Å)	$Fe_{a3}-N_1$† (Å)	Cu_B-N_3† (Å)	$Fe_{a3}-Cu_B$ (Å)
I	2.07‡	1.90‡	2.02	1.87	5.22
II	2.07		1.98	2.44	5.18
III		1.90	2.79	1.75	5.13

† N_1 and N_3 are the terminal N atoms of an azide molecule. ‡ These distances are the distances in the analogous structures in myoglobin azide (Mattevi *et al.*, 1991) and in an azide derivative of ascorbate oxidase (Messerschmidt *et al.*, 1993).

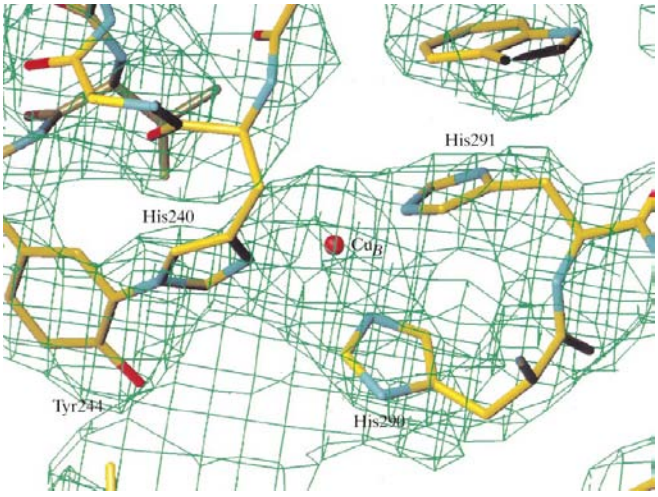

Figure 1
A 2.9 Å MIR/*DM* electron-density map of the Cu_B site drawn at the 2σ level. Three histidine residues and a covalent bond between Tyr244 and His240 are superposed on the map.

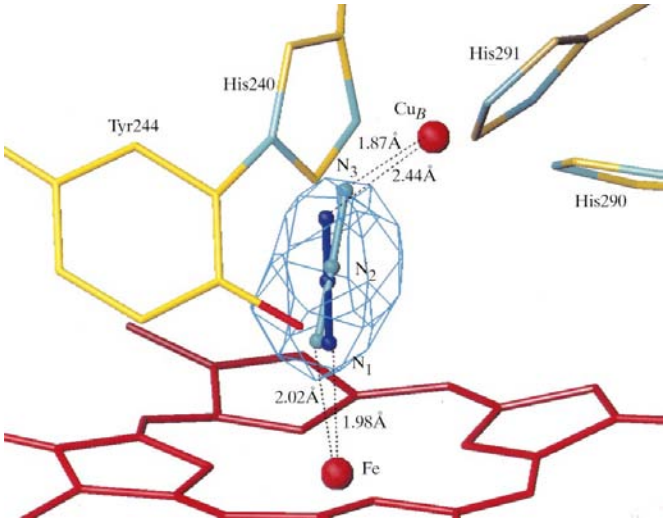

Figure 2
A difference electron-density map for the azide bound at the O_2-reduction site. The electron-density cage is drawn at the 4σ level. Haem a_3 and Cu_B are depicted by red sticks and red spheres, respectively. The two structural models of azide obtained by the refinement are also shown in the electron-density cage. Models I and II given in Table 2 are colored light blue and dark blue, respectively.

3.6. Conformation of a polypeptide segment from Gly49 to Asn55 in subunit I

The atomic model of the Gly49–Asn55 segment of the fully oxidized form was used as an initial model in the refinement of the structure of the Gly49–Asn55 segment of the azide-bound fully oxidized form. After refinement with *X-PLOR*, the model was superposed on the MIR/*DM* map of azide-bound fully oxidized cytochrome *c* oxidase. The resulting atomic model indicates the conformation of the Gly49–Asn55 segment to be identical to that of the fully oxidized form. When the model of the fully reduced form was used as an initial structure in simulated-annealing refinement coupled with positional refinement and *B*-factor refinement using *X-PLOR*, the initial model was converted to a model identical to that of the oxidized form within experimental accuracy. This indicates that the electron density of the azide-bound fully oxidized form is accurate enough to differentiate the conformation of the Gly49–Asn55 segment in the fully oxidized form from that in the fully reduced form.

4. Discussion

Azide is a potent inhibitor of cytochrome *c* oxidase. The effects of this reagent on the enzyme have been studied for almost 60 years since the pioneering work of Keilin & Hartree (1939). Both cyanide and azide are considered to bind to haem a_3 in the oxidized state (Ferguson-Miller & Babcock, 1996; Keilin & Hartree, 1939). A very small but fairly rapid change in the visible–Soret absorption spectrum of the fully oxidized enzyme is induced by azide (Wever *et al.*, 1973; Yoshikawa & Caughey, 1992; Li & Palmer, 1993), while cyanide induces a marked change in the absorption spectrum at very slow rate (Yoshikawa & Orii, 1973; Van Buuren *et al.*, 1972).

Infrared studies have revealed many unique features of the azide's reaction with the enzyme (Yoshikawa & Caughey, 1992; Li & Palmer, 1993). Azide produces two sharp infrared bands at 2051 and 2041 cm^{-1} for the fully oxidized enzyme. The 2041 cm^{-1} band splits into two bands at 2035 and 2024 cm^{-1} on replacing $^{14}N-^{14}N-^{14}N$ with $^{15}N-^{14}N-^{14}N$,

while the 2051 cm^{-1} band is shifted to 2039 cm^{-1} without band splitting by the isotopic replacement. Thus, the azide binding giving the 2051 cm^{-1} band seems significantly less specific than that giving the 2041 cm^{-1} band. However, both bands were removed by cyanide (Yoshikawa & Caughey, 1992). The effect of pH on the inhibitory effect of azide indicates that HN_3, not N_3^-, reacts with the enzyme to inhibit the enzymatic activity (Stannard & Horecker, 1948). The azide molecule, HN_3, should give an infrared band around 2140 cm^{-1} (McCoy & Caughey, 1970). Therefore, both the 2051 and 2041 cm^{-1} bands must arise from N_3^-. In other words, HN_3 molecules bind to the enzyme to form N_3^- compounds. Therefore, proton-accepting sites are likely to be near the azide-binding sites.

The present crystallographic results improve the understanding of the reaction of azide with the enzyme in the fully oxidized state. The 2051 cm^{-1} band, which provides a single isotopically shifted band at 2039 cm^{-1} for $^{15}N-^{14}N-^{14}N$, is likely to arise from the azide interacting with Asn422 and Tyr379. These interactions (hydrogen bonding) could be too weak to split the isotopically shifted azide band. The band position is close to that arising from free azide anion in solution at 2047 cm^{-1}, but the band width is much narrower than that of the free azide anion (Yoshikawa & Caughey, 1992). This infrared property seems to be consistent with the hydrogen-bonding interactions of azide with Asn422 and Tyr379. The sharp 2041 cm^{-1} band must arise from the azide ion bound at Fe_{a3}^{3+}. At the present resolution, both bridging and terminal binding geometries are equally possible, as described above. Azide bridged between two different metals is unlikely to be in a symmetric coordination. Therefore, both geometries would provide a splitting isotopic shift for $^{15}N-^{14}N-^{14}N$. The 2041 cm^{-1} band is as intense as the 2051 cm^{-1} band (Yoshikawa & Caughey, 1992). This result strongly suggests the terminal coordination geometry for the 2041 cm^{-1} band, since μ-1,3 coordination is likely to provide a much less intense infrared band than terminal coordination. In other words, the infrared results are definitely more consistent with terminal coordination than μ-1,3 coordination.

Li & Palmer (1993) carefully examined the small absorbance changes induced by azide, showing two azide-binding sites with K_d values of 64 μM and 20 mM at pH 8.0, respectively. Under the present conditions for preparation of crystals of the azide-bound enzyme (5 mM azide at pH 6.8), both binding sites are likely to be occupied, since azide binding is greatly enhanced at lower pH. The infrared results of Li & Palmer (1993) indicate that azide at the high-affinity site has an infrared band at 2051 cm^{-1}. The azide binding to Fe_{a3}^{3+} giving the 2041 cm^{-1} band may be influenced strongly by pH, so that K_d for the 2041 cm^{-1} band is larger than that for the 2051 cm^{-1} band at pH 8.0 under the conditions of Li & Palmer (1993). The azide ion at the non-metal site seems to influence the absorption spectrum of the haems, although very weakly.

The azide-binding site on the transmembrane surface (Tyr379 and Asn422) is covered with detergent molecules. Therefore, HN_3 approaches the site much more readily than N_3^-. His429 near the non-metal site for azide binding could serve as a proton-accepting site for HN_3. The proton-accepting site for the azide bound at haem a_3 could be Tyr244 or the imidazole of His290 or His291. His240 is unable to accept protons because of its covalent bond to Tyr244.

Infrared results indicated that only one equivalent of cyanide binds quantitatively to the fully oxidized enzyme (Yoshikawa & Caughey, 1992). One equivalent of cyanide, as stated above, removes both the 2051 cm^{-1} band and the 2041 cm^{-1} band (Yoshikawa & Caughey, 1992). The cyanide-binding site is very likely to be Fe_{a3}^{3+}. Thus, cyanide binding at Fe_{a3}^{3+} anticooperatively removes the azide at the site composed of Asn422 and Tyr379 in the transmembrane surface. These two amino acids and His429, the possible proton-accepting site, are highly conserved among mitochondrial cytochrome *c* oxidases (Bairoch & Apweiler, 1999). Therefore, this azide-binding site could provide a regulatory mechanism by a negatively charged substance.

The cross-linked structure between His240 and Tyr244 is detectable in all crystal structures of bovine heart cytochrome *c* oxidase so far obtained (Yoshikawa *et al.*, 1998). Furthermore, the cross-linked structure has not been influenced by the time and conditions of storage of the crystals. Therefore, the cross linking is likely to be produced by a physiologically programmed post-translational modification.

The conformation of Asp51 seems to be determined by the oxidation state of the metal sites and not by the ligand-binding state, since both azide and CO do not influence the conformation (Yoshikawa *et al.*, 1998). The results suggest that the O_2-reduction site does not control the conformation of Asp51. Thus, the oxidation states of Cu_A and haem *a* may control the conformation. It has been suggested that protons are pumped by the conformational change in Asp51 (Yoshikawa *et al.*, 1998). Redox changes in Cu_A and haem *a* should therefore be coupled to the proton pumping in this enzyme. Coupling of the oxidation state of haem *a* with proton pumping has been proposed (Capitanio *et al.*, 1997). However, different mechanisms may be possible for controlling the conformational change in Asp51 in other oxidation and ligand-binding states of the O_2-reduction sites, such as in the ferryl state of Fe_{a3} during catalytic turnover.

The fully oxidized bovine heart cytochrome *c* oxidase as isolated is alternatively known as the resting oxidized form, since it is not involved in the enzymic cycle (Antonini *et al.*, 1977). Both electron transfer (Antonini *et al.*, 1977) and cyanide binding (Yoshikawa & Orii, 1974; Jones *et al.*, 1984) to haem a_3 in the fully oxidized form under turnover conditions are much faster than in the resting oxidized form, suggesting a difference in the ligand-binding structure at the O_2-reduction site. However, the conformation of Asp51 in the fully oxidized enzyme under turnover conditions is likely to be the same as that in the resting oxidized form, since the difference between the two forms is in the ligand-binding structure at the O_2-reduction site.

According to Iwata *et al.* (1995), bacterial cytochrome *c* oxidase in the fully oxidized azide-bound form lacks one of the imidazole ligands of Cu_B. However, our azide-bound form clearly shows all the three imidazoles in the Cu_B site. That is, it does not support the histidine-cycle mechanism. This discre-

pancy must indicate an evolution in the conformational stability of one of the imidazole ligands of Cu_B.

This research was supported in part by Grants-in-Aid for Scientific Research on Priority Areas (Molecular Science on the Specific Roles of Metal Ions in Biological Functions to SY and Nos. 06276102 and 05244102 to TT), Grants-in-Aid for Scientific Research (No. 40068119 to SY and No. 06558102 to TT) from the Ministry of Education and Culture of Japan and Grant-in-Aid for 'Research for the Future' Program from the Japan Society for the Promotion of Science (JSPS-RFTF96L00503 to TT) and was performed with the approval of the Photon Factory Advisory Committee, the National Laboratory for High Energy Physics, Japan (proposal Nos. 91-050 and 94G-041). We thank Drs N. Sakabe, A. Nakagawa, N. Watanabe and S. Ikemizu for their expert help with data collection using the Weissenberg camera and synchrotron radiation. TT and SY are members of the TARA project of Tsukuba University.

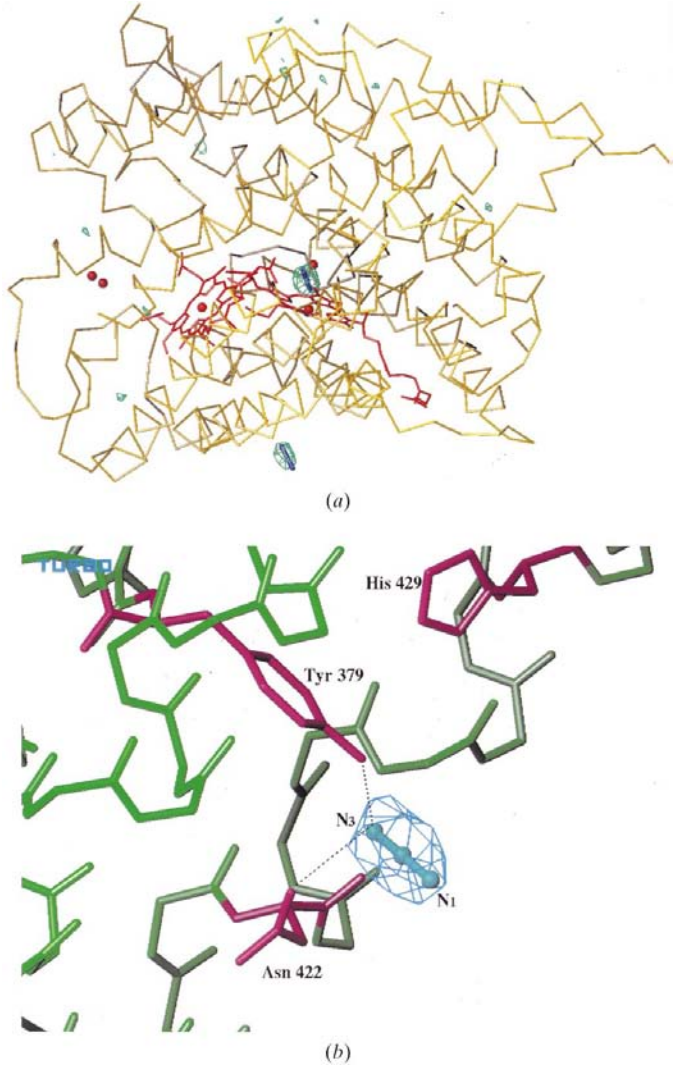

Figure 3
The electron density of the azide bound at the non-metal site. (*a*) A ($F_o - F_c$) difference Fourier map showing the two azide-binding sites. The map is shown at the 4σ level. The C^{α} backbone of subunit I is shown in yellow, two haems and three Cu atoms are shown in red and azide molecules are shown in cyan. (*b*) A close-up of the azide at the non-metal site. The structures of Tyr379, Asn422 and His429 are shown in purple and the backbone of subunit I is shown in green.

References

Antonini, E., Brunori, M., Colosimo, A., Greenwood, C. & Wilson, M. T. (1977). *Proc. Natl Acad. Sci. USA*, **74**, 3128–3132.
Argos, P. & Rossmann, M. G. (1976). *Acta Cryst.* B**32**, 2975–2979.
Bairoch, A. & Apweiler, R. (1999). *Nucleic Acids Res.* **27**, 49–54.
Brünger, A. T. (1992). *Nature (London)*, **355**, 472–475.
Brünger, A. T., Kuriyan, J. & Karplus, M. (1987). *Science*, **235**, 458–460.
Buehner, M., Ford, G. C., Moras, D., Olsen, K. W. & Rossmann, M. G. (1974). *J. Mol. Biol.* **82**, 563–585.
Capitanio, N., Vygodina, T. V., Capitanio, G., Konstantinov, A. A., Nicholls, P. & Papa, S. (1997). *Biochim. Biophys. Acta*, **1318**, 255–265.
Collaborative Computational Project, Number 4 (1994). *Acta Cryst.* D**50**, 760–763.
Engh, R. A. & Huber, R. (1991). *Acta Cryst.* A**47**, 392–400.
Ferguson-Miller, S. & Babcock, G. T. (1996). *Chem. Rev.* **96**, 2889–2907.
Green, D. W., Ingram, V. M. & Perutz, M. F. (1954). *Proc. R. Soc. London Ser. A*, **225**, 287–307.
Iwata, S., Ostermeier, C., Ludwig, B. & Michel, H. (1995). *Nature (London)*, **376**, 660–669.
Jones, M. G., Bickar, D., Wilson, M. T., Brunori, M., Colosimo, A. & Sarti, P. (1984). *Biochem. J.* **220**, 57–66.
Kadenbach, B., Ungibauer, M., Jarausch, J., Büge, U. & Kuhn-Nentwig, L. (1983). *Trends Biochem. Sci.* **8**, 398–400.
Keilin, D. & Hartree, E. F. (1939). *Proc. R. Soc. London Ser. B*, **127**, 167–191.
Li, W. & Palmer, G. (1993). *Biochemistry*, **32**, 1833–1843.
McCoy, S. & Caughey, W. S. (1970). *Biochemistry*, **9**, 2387–2393.
Mattevi, A., Gatti, G., Coda, A., Rizzi, M., Ascenzi, P., Brunori, M. & Bolognesi, M. (1991). *J. Mol. Recognit.* **4**, 1–6.
Matthews, B. W. (1968). *J. Mol. Biol.* **33**, 491–497.
Messerschmidt, A., Luecke, H. & Huber, R. (1993). *J. Mol. Biol.* **230**, 997–1014.
Morris, A. L., MacArthur, M. W., Hutchinson, E. G. & Thornton, J. M. (1992). *Proteins Struct. Funct. Genet.* **12**, 345–364.
Otwinowski, Z. (1991). *Proceedings of the CCP4 Study Weekend. Isomorphous Replacement and Anomalous Scattering*, edited by W. Wolf, P. R. Evans & A. G. W. Leslie, pp. 80–86. Warrington: Daresbury Laboratory.
Otwinowski, Z. & Minor, W. (1997). *Methods Enzymol.* **276**, 307–326.
Ramachandran, G. N. & Sasisekharan, V. (1968). *Adv. Protein Chem.* **23**, 283–437.
Sakabe, N. (1983). *J. Appl. Cryst.* **16**, 542–547.
Stannard, J. N. & Horecker, B. L. (1948). *J. Biol. Chem.* **172**, 599–608.
Tsukihara, T., Aoyama, H., Yamashita, E., Tomizaki, T., Yamaguchi, H., Shinzawa-Itoh, K., Nakashima, R., Yaono, R. & Yoshikawa, S. (1995). *Science*, **269**, 1069–1074.
Tsukihara, T., Aoyama, H., Yamashita, E., Tomizaki, T., Yamaguchi, H., Shinzawa-Itoh, K., Nakashima, R., Yaono, R. & Yoshikawa, S. (1996). *Science*, **272**, 1136–1144.
Van Buuren, K. J. H., Nichols, P. & Van Gelder, B. F. (1972). *Biochim. Biophys. Acta*, **256**, 258–276.
Wang, B.-C. (1985). *Methods Enzymol.* **115**, 90–112.
Warburg, O. (1924). *Biochem. Z.* **152**, 479–494.
Wever, R., Muijsers, A. O. & Van Gelder, B. F. (1973). *Biochim. Biophys. Acta*, **325**, 8–15.

Wikström, M., Bogachev, A., Finel, M., Morgan, J. E., Puustinen, A., Raitio, M., Verkhovskaya, M. & Verkhovsky, M. I. (1994). *Biochim. Biophys. Acta*, **1187**, 106–111.
Yoshikawa, S. & Caughey, W. S. (1992). *J. Biol. Chem.* **267**, 9757–9766.
Yoshikawa, S. & Orii, Y. (1973). *J. Biochem. (Tokyo)*, **73**, 637–645.
Yoshikawa, S. & Orii, Y. (1974). *J. Biochem. (Tokyo)*, **76**, 271–281.
Yoshikawa, S., Shinzawa-Itoh, K., Nakashima, R., Yaono, R., Yamashita, E., Inoue, N., Fei, M. J., Peters-Libeu, C., Mizushima, T., Yamaguchi, H., Tomizaki, T. & Tsukihara, T. (1998). *Science*, **280**, 1723–1729.
Zhang, K. Y. J. & Main, P. (1990). *Acta Cryst.* A**46**, 377–381.